JOURNAL OF SOLID STATE CHEMISTRY 84, 211–225 (1990)

II. Structural Aspects of the α Transition in Off-Stoichiometric $Fe_{1-x}S$ Crystals

F. KELLER-BESREST* AND G. COLLIN

Unité associée au CNRS No. 200, Université René Descartes, 4 avenue de l'Observatoire, 75006 Paris, France

Received March 15, 1988; in revised form July 12, 1989

Study of the α transition in the $Fe_{1-x}S$ system (NiAs-type solid solution) is completed by structural analysis versus temperature of the cation-deficient crystals $Fe_{0.985}S$ and $Fe_{0.975}S$. The influence of x and T on the disorder phenomena and on the gradual change of the cationic lattice is analyzed in the LT hexagonal $\sqrt{3}a,2c$ phase (a and c are NiAs-type substructure lattice constants). The hypothesis of the existence of an S^{-1} impurity level in the band gap of FeS, originating from the formation of covalent pairs $(S–S)^{2-}$ around each vacancy, leads to a model of conductivity by polarons. This accounts for the decrease with x in the transition energy. The transition is suppressed for $x = 0.05$, which corresponds to the critical polaron concentration beyond which the polaron gas becomes degenerate.

I. Introduction

A previous paper (*1*) has been devoted to some structural aspects of the α transition in the $Fe_{1-x}S$ system. The present paper reports structural analyses of $Fe_{0.985}S$ and $Fe_{0.975}S$ crystals. The results establish a similarity in the behavior of iron-deficient or M-substituted materials (M = Cr, Mn, Co in $Fe_{1-x}M_xS$) (*2, 3*). This allows the polaron model of the mechanism of transition to be extended to the $Fe_{1-x}S$ system.

II. Qualitative X-Ray Study of $Fe_{1-x}S$ Crystals

Samples were prepared as described in Ref. (*1*). The variations with T of the a and c substructure lattice constants of FeS, $Fe_{0.985}S$, and $Fe_{0.975}S$ are reported in Fig. 1. At the transition, one observes opposite changes in a and c, and an important discontinuity in c that becomes weaker and less abrupt as x increases.

Previous studies (*1, 4*) showed that the iron-poor part of the phase diagram ($x_{lim} = 0.05 < x \leq 0.125$ (= Fe_7S_8)) is the domain of existence of various apparently hexagonal superstructures $2a,nc$ associated with different vacancy orderings. The presumption is that the two-phase mixture observed in $Fe_{1-x}S$ powders in the transition range also exists in crystals and corresponds to the progressive formation of $2a,nc$-type ordering in off-stoichiometric domains coexisting with stoichiometric FeS $\sqrt{3}a,2c$ domains. This is confirmed on Weissenberg diagrams of a $Fe_{0.965}S$ crystal at different temperatures. Reflections from a $2a,2a,nc$ lattice are observed as well as those from the

* To whom all correspondence should be addressed.

0022-4596/90 $3.00

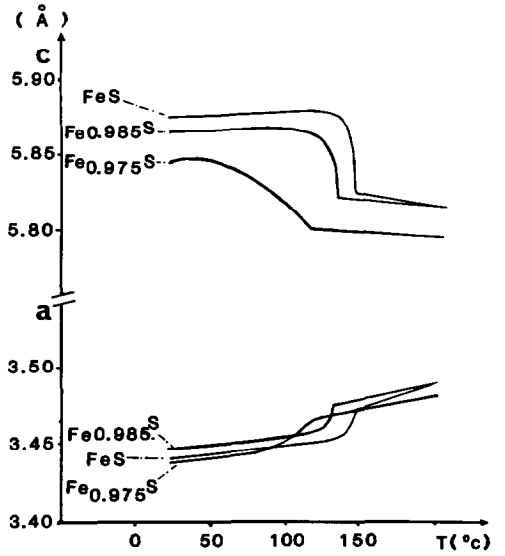

FIG. 1. Variation with T of the substructure lattice constants a and c of FeS, $Fe_{0.985}S$, $Fe_{0.975}S$ crystals, around the α transition.

$\sqrt{3}a,2c$ lattice. At room temperature they are weak and diffuse, and the $00l$ diffraction spots are split; but the disorder increases with T (Fig. 2). The hysteresis of the transition is very important (40°C) and the initial crystallographic state detected before heating is recovered after 2 weeks.

The segregation of vacancies in disordered domains where the triangular Fe clusters of the LT $\sqrt{3}a,2c$ superstructure are cleaved has been discussed in Part I (Section IVB). Referring to the plot of c versus x (Part I), the coexistence of these domains of different composition explains the splitting of the $00l$ reflections.

In the previous FeS study, one observed that the shortening of the correlation length of the $\sqrt{3}a,2c$ superstructure associated with the relaxation of the atomic shifts was induced by the temperature only. But vacancies also play an equivalent part in the breaking up of this lattice. This is confirmed by qualitative structural analysis performed on $Fe_{0.985}S$ and $Fe_{0.975}S$ crystals, as with the FeS crystal (results summarized in Fig. 3). The intensity ratio I/I_0 and the peak profile of characteristic reflections are presented in Figs. 4 and 5.

The shoulders on the $00l$ (a,c) peaks of $Fe_{0.985}S$ and $Fe_{0.975}S$ at RT establish that already for $x \geq 0.015$ the crystals are diphasic (Figs. 4c, 5c, and 5d).

Comparison of the $121(\sqrt{3}a,2c)$ peaks of FeS, $Fe_{0.985}S$ and $Fe_{0.975}S$ shows that when x increases, the I/I_0 ratio versus T decreases more rapidly to zero, and, at a given temperature, the peak width increases. This indicates that the disordered state of a crystal increases with x and/or T. As previously observed in FeS, the NiAs lattice distortion relaxes in the small $\sqrt{3}a,2c$ domains which remain. But in the highly disordered pretransition state of $Fe_{0.975}S$, the spectacular increase in the $110(a,c)$ reflection originates mainly from the majority disordered domains where the relaxation is almost complete.

The kinetics of the crystallographic hysteresis is followed by the $031(2a,c)$ reflection of $Fe_{0.985}S$. At $T_\alpha - 4°C = 128°C$, the $2a,c$ superstructure (unsuitably named a HT modification) is long-range ordered (Fig. 4e). When this temperature is held steady, the $031(2a,c)$ reflection progressively decreases, while simultaneously the previously absent LT $121(\sqrt{3}a,2c)$ reflection appears and strengthens. Its initial intensity value, recorded at RT before heating, returns after about 15 h.

The absence of shoulders on the $00l$

FIG. 2. The $h0l$ level of the $Fe_{0.965}S$ crystal. (a) At RT the crystal is diphased. Long-range-ordered $\sqrt{3}a,2c$ domains give sharp superstructure reflections, while those from a short-range-ordered $2a,2a,nc$ lattice are weak and diffuse. (b) At 50°C. Both kinds of superstructure spots are diffuse. The split of the $00l$ reflections disappears (high disorder state). (c) At $T_\alpha = 102°C$, at the transition, only the substructure reflections remain.

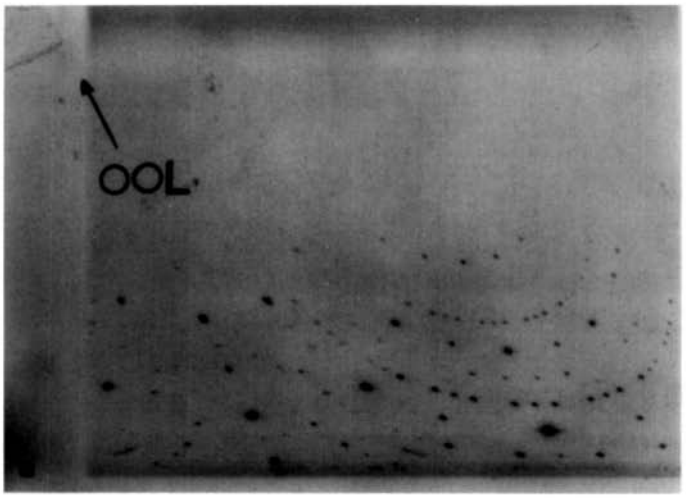
OOL

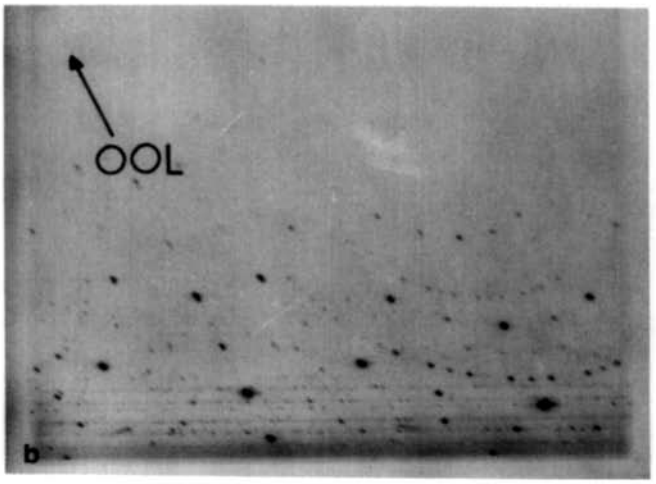
OOL
b

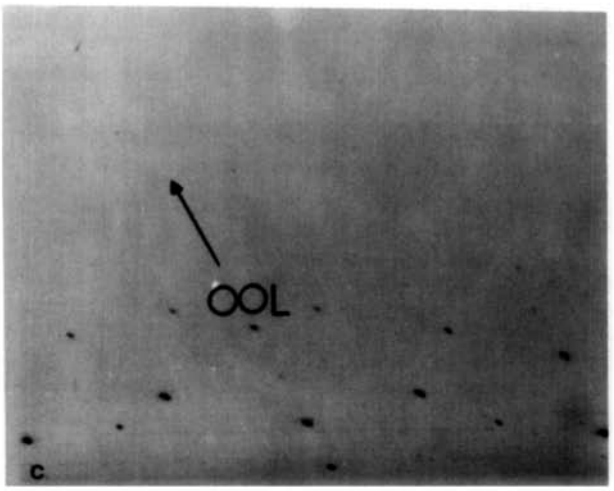
OOL
c

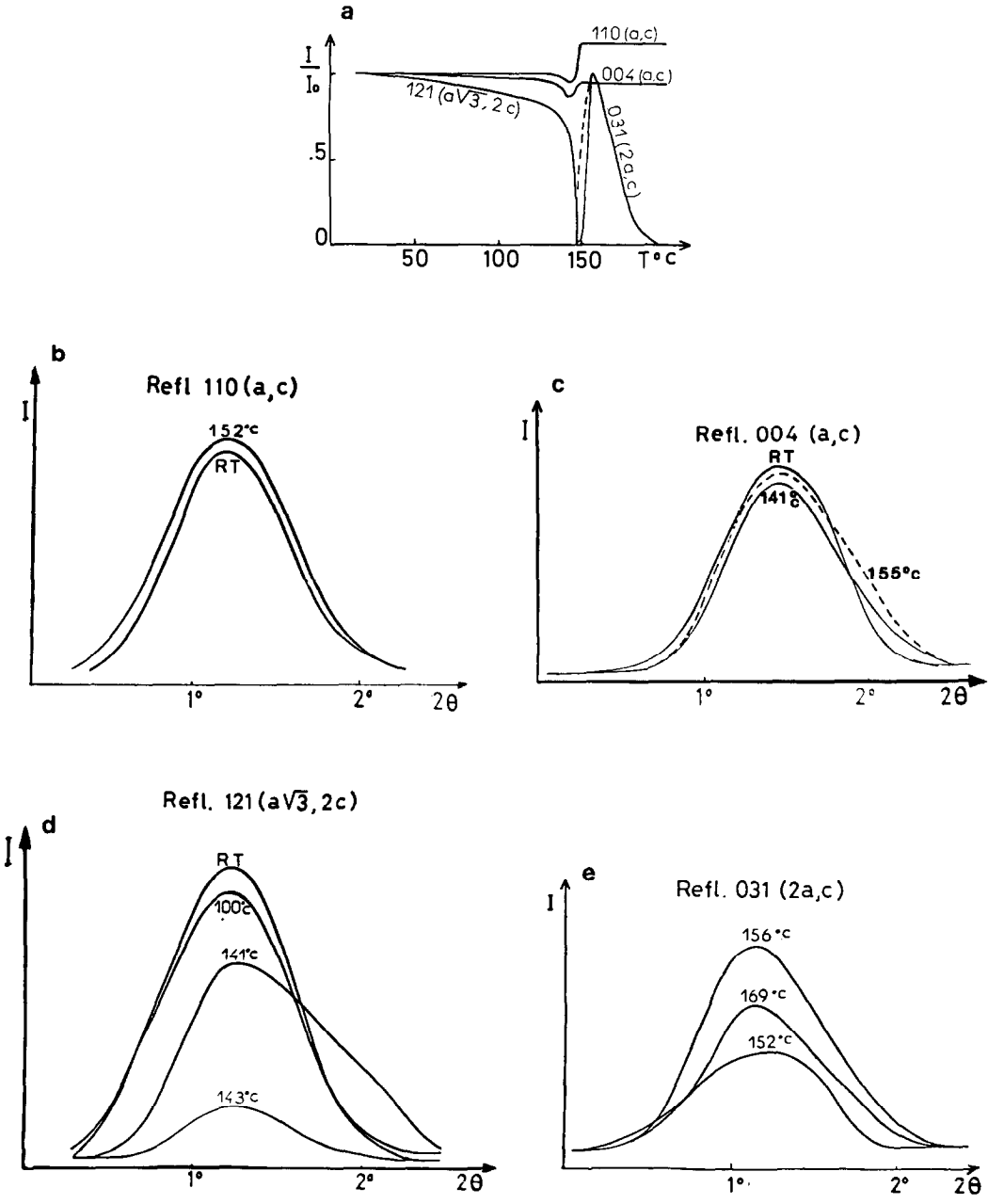

FIG. 3. Evolution with T of the structural characteristics of the FeS crystal (T_α = 147°C; hysteresis = 4°C). Dotted lines: observations in the hysteresis range. (a) Relative intensity I/I_0 of reflections 110(a,c) and 004(a,c) from the substructure, and 121($\sqrt{3}a$,2c) and 031(2a,c) from respectively the LT and HT superstructures. (b and c) Peak profiles of substructure reflections: 110(a,c) and 004(a,c). (d) Peak profiles of LT superstructure reflection 121($\sqrt{3}a$,2c). (e) Peak profiles of HT superstructure reflection 031(2a,c).

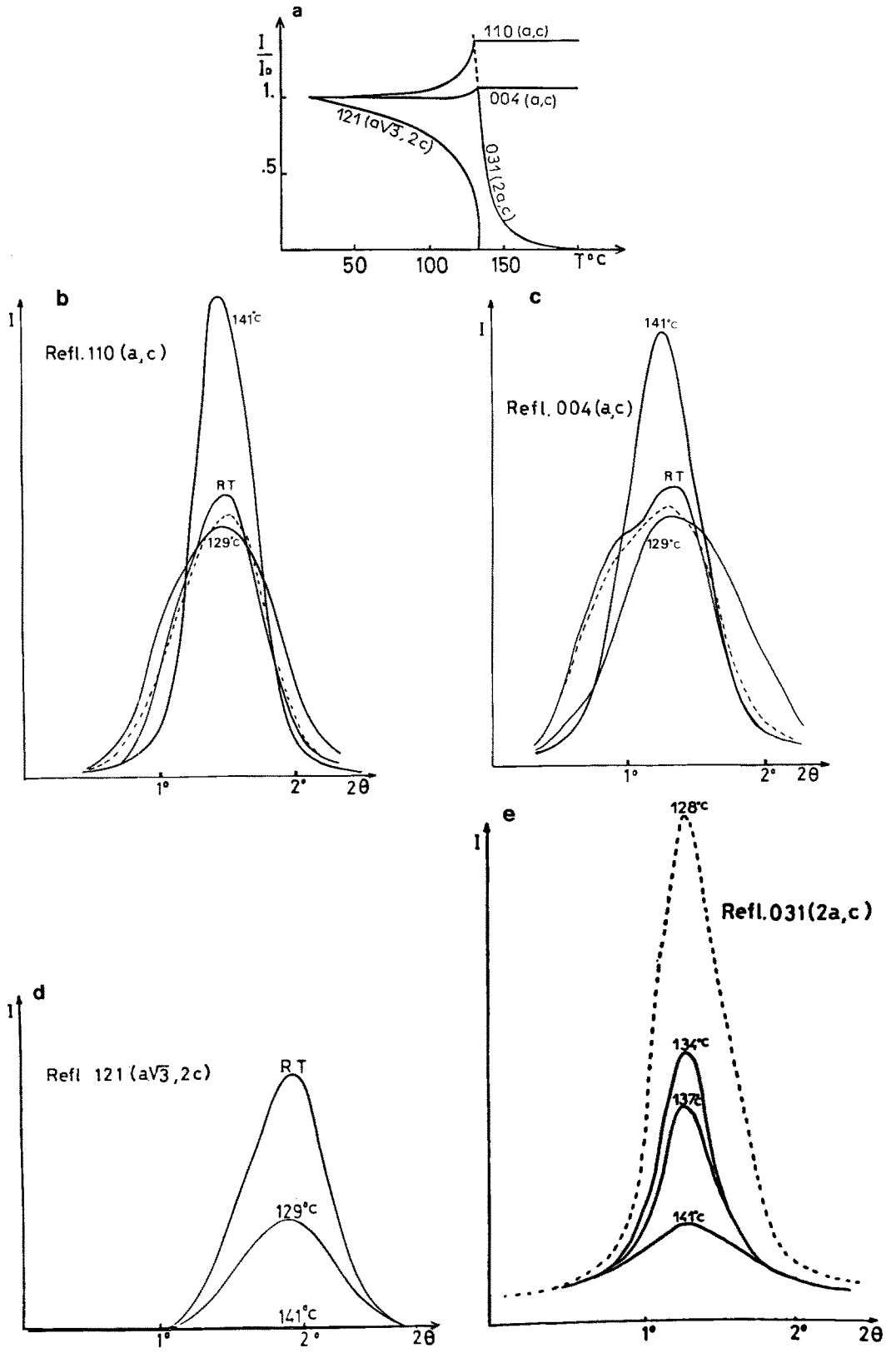

FIG. 4. As in Fig. 3, but for $Fe_{0.985}S$ (T_α = 132°C; hysteresis = 20°C).

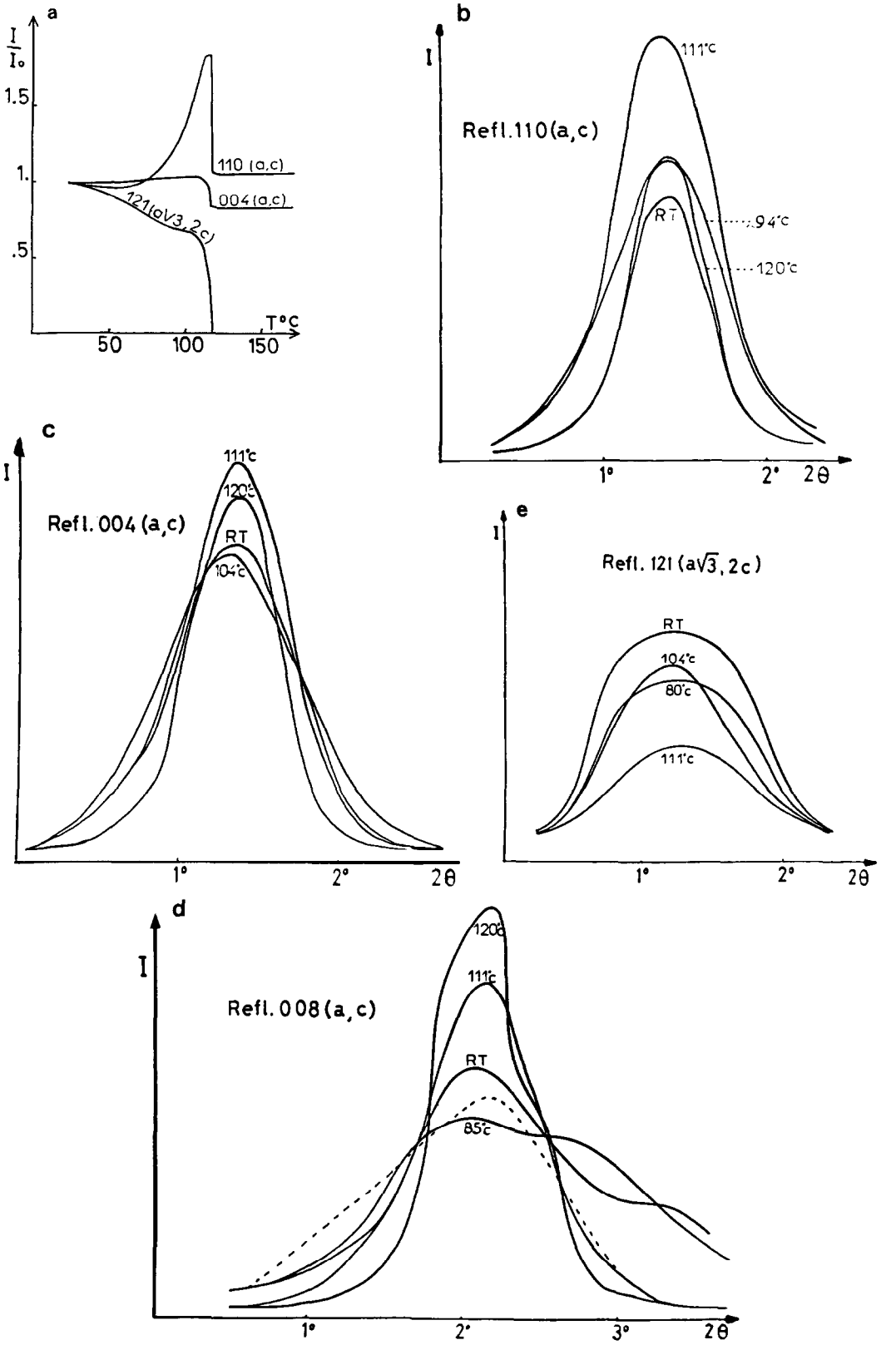

FIG. 5. (a) As in Fig. 3, but for $Fe_{0.975}S$ (T_α = 116°C; hysteresis = 28°C). (b, c, and d) Peak profiles of respectively 110(a,c); 004(a,c); 008(a,c) substructure reflections. (e) Peak profiles of the LT superstructure reflection 121($\sqrt{3}a$,2c).

peaks at HT indicates that the $2a,c$ modification accepts statistically disordered or short-range-ordered vacancies in its lattice. Under these conditions, the HT–LT transition appears to be a diffusion of vacancies from a statistical disorder at HT to a segregation in off-stoichiometric domains at LT. Because of the slow kinetics of the diffusion, hysteresis increases quickly with x, as observed on powders and crystals.

The $2a,c$ modification is no longer observable in HT $Fe_{0.975}S$, and the change of the I/I_0 ratio of $110(a,c)$ and $004(a,c)$ reflections is different from the change observed in FeS and $Fe_{0.985}S$. For these crystals, the existence of the $2a,c$ modification, which is a weak NiAs lattice distortion, leads to an increase in the $110(a,c)$ reflection and the slight change of $004(a,c)$. The unknown HT phase of $Fe_{0.975}S$ is associated with the "metallic" state of the compound.

Referring to the phase diagram of the $Fe_{1-x}S$ system (*1*, *4*), the metallic range is composed of two parts:

—The first, which is independent of temperature, corresponds to the iron-poor side of the system ($x_{lim} = 0.05 \leq x \leq 0.125$), characterized by the existence of various apparently hexagonal $2a,nc$ superstructures.

—The other, in the α transition range ($0 \leq x \leq x_{lim} = 0.05$) corresponds to the HT state. For $x \leq 0.015$, it is associated with the $2a,c$ modification which can be considered an element of the $2a,nc$ superstructures series. But the structural type is unknown for x values between 0.015 and $x_{lim} = 0.05$ which mark the border with the $2a,nc$ structural range.

Previous studies (*4*) showed that the x-induced transitions between these $2a,nc$ structural types, with different n values, correspond to the change of a partial vacancy ordering into a long-range ordering. In the composition range where the HT structural type is unknown, one supposes that a new partial ordering occurs in the $2a,c$ modification and gives rise to a $2a,nc$-type short-range ordering. The structural analysis of hexagonal $2a,3c$ Fe_7S_8 ($x = 0.125$) (*5*) shows that, compared to the pure NiAs packing, this ordering leads to important cation shifts in the hexagonal plane and parallel to the c direction. Such a NiAs lattice distortion would account for the decrease in the I/I_0 ratio of the substructure reflections observed at $T > T_\alpha$ for $Fe_{0.975}S$. The conclusion is that from x close to 0.025, the HT metallic state is now associated with a $2a,nc$ structural type, but with a limited correlation length which makes X-ray identification difficult.

From these observations performed on iron-deficient compounds, one can conclude by comparison with FeS:

—The disorder mechanism of the transition (induced by temperature only in FeS) is increased because of vacancies which act parallel to temperature.

—Vacancies contribute to the breaking up of the $\sqrt{3}a,2c$ domains and this explains the lowering of the energy of the transition. This transition occurs in the minority $\sqrt{3}a,2c$ domains which remain, with relaxed Fe clusters.

III. Structural Analysis vs Temperature

(*A*) *Refinements*

As in Part I, the LT $\sqrt{3}a,2c$ cell (SG $P\bar{6}2c$) is studied at RT and in the pretransition range. But only for the $Fe_{0.985}S$ composition can the HT $2a,c$ modification (SG $P6_3mc$) be analyzed above the transition. The reflections are collected between $2\theta = 0°$ and 65° in two hexagonal sectors. After the absorption correction, the arithmetic means of the data are used in the refinement, including those of zero intensity. As explained in Part I, the coexistence of ordered ($\sqrt{3}a,2c$ or $2a,c$) and disordered domains requires treating sub- and super-

structure reflections with two independent scale factors (SC). However, the refinement of the $\sqrt{3}a,2c$ cell of $Fe_{0.975}S$ at $T_\alpha - \Delta T = 110°C$ needed special treatment. A first stage based on the whole set of reflections gives a final R factor of 9.3%, decomposed into partial Rs of 6% for the substructure reflections and 13.3% for the superstructure reflections. The superstructure scale factor is then 60(± 6.4)% smaller than the substructure scale factor. This difference, which measures the percentage of disordered domains, tends to remove substructure reflections from the refinement. The most important part of their intensity comes from the disordered domains with almost ideal NiAs lattice, and the substructure reflection intensity ought to be calculated as I = SC(substructure)$(F^2(\sqrt{3}a,2c) + t \times F^2(a,c))$. But t, which measures the proportion of disordered domains in the crystal, cannot be determined independently of SC(substructure).

When based on superstructure reflections only, the first cycles of refinement exhibit a high correlation between the position parameter x and the anisotropic thermal parameters β_{11}, β_{12}, and β_{22} of Fe and S_3 atoms, corresponding to their delocalization in the hexagonal plane. For each atom, β_{12} is then fixed at the value obtained. This gives with β_{11} and β_{22} an anisotropic ther-

TABLE I

FINAL PARAMETERS OF REFINEMENTS OF LT $\sqrt{3}a,2c$ STRUCTURES OF $Fe_{0.985}S$ AND $Fe_{0.975}S$ CRYSTALS AT RT AND JUST BELOW T_α

Position $P\bar{6}2C$	Position ideal NiAs	$Fe_{0.985}S$		$Fe_{0.975}S$	
		RT	116°C	RT	110°C
Fe (12*i*)					
x	$\frac{1}{3}$	0.3781(2)	0.3735(4)	0.3716(4)	0.3724(6)
y	0	0.0543(2)	0.0492(4)	0.0479(4)	0.0478(7)
z	$\frac{1}{8}$	0.1231(1)	0.1232(2)	0.1232(2)	0.1235(2)
S_1 (2*a*)					
x	0	0	0	0	0
y	0	0	0	0	0
z	0	0	0	0	0
S_2 (4*f*)					
x	$\frac{1}{3}$	$\frac{1}{3}$	$\frac{1}{3}$	$\frac{1}{3}$	$\frac{1}{3}$
y	$\frac{2}{3}$	$\frac{2}{3}$	$\frac{2}{3}$	$\frac{2}{3}$	$\frac{2}{3}$
z	0	0.0200(2)	0.0180(6)	0.0188(5)	0.0145(7)
S_3 (6*h*)					
x	$\frac{2}{3}$	0.6645(4)	0.6654(9)	0.6640(9)	0.6604(9)
y	0	−0.0028(4)	−0.0027(9)	−0.0030(9)	−0.0012(9)
z	$\frac{1}{4}$	$\frac{1}{4}$	$\frac{1}{4}$	$\frac{1}{4}$	$\frac{1}{4}$
Total R		3.1%	5.7%	6.15%	—
nb of reflections		285	279	281	—
Partial R and *nb* of reflections in parenthesis					
Substructure		2.2%(55)	3.5%(55)	3.1%(55)	—
Superstructure		3.9%(230)	7.7%(224)	8.8%(226)	8.1%(228)
Substructure lattice constants in Å					
a		3.444(1)	3.461(1)	3.441(1)	3.464(1)
c		5.872(1)	5.863(1)	5.830(1)	5.810(1)

TABLE II

ANISOTROPIC TEMPERATURE FACTORS (Å² × 10⁴) IN LT $\sqrt{3}a,2c$ STRUCTURE OF $Fe_{0.985}S$ AND $Fe_{0.975}S$ CRYSTALS AT RT AND JUST BELOW T_α

	$Fe_{0.985}S$		$Fe_{0.975}S$	
Atoms	RT	116°C	RT	110°C
Fe				
U_{11}	168(5)	225(10)	159(10)	165(5)
U_{22}	148(5)	202(10)	125(10)	184(7)
U_{33}	152(3)	243(5)	197(5)	482(16)
U_{12}	91(4)	147(8)	92(8)	111[a]
U_{13}	1(3)	−3(9)	−9(7)	8(8)
U_{23}	−9(3)	−13(10)	−5(7)	−4(8)
S_1				
$U_{11} = U_{22}$	87(8)	154(18)	41(14)	49(18)
U_{33}	146(12)	217(30)	168(24)	122(30)
$U_{12} = 0.5\ U_{11}$				
$U_{13} = U_{23}$	0	0	0	0
S_2				
$U_{11} = U_{22}$	94(6)	131(12)	80(11)	151(22)
U_{33}	142(9)	248(22)	217(22)	140(17)
$U_{12} = 0.5\ U_{11}$				
$U_{13} = U_{23}$	0	0	0	0
S_3				
U_{11}	82(8)	170(19)	76(15)	253(41)
U_{22}	72(7)	130(16)	96(16)	241(41)
U_{33}	174(9)	217(18)	153(12)	379(50)
U_{12}	37(7)	70(16)	46(15)	117[a]
$U_{13} = U_{23}$	0	0	0	0

[a] Values fixed after the first cycles of the only superstructure refinement.

mal motion which is comparable to the results obtained on FeS and $Fe_{0.985}S$ just below T_α. Under these conditions, the R factor for superstructure reflections decreases from 13.3 to 8.1%.

The results of refinement of the LT $\sqrt{3}a,2c$ phases at RT and below the transition (at $T_\alpha - \Delta T$) are presented in Table I. Anisotropic temperature factors are reported in Table II. Table III presents the final parameters and R value for the HT $2a,c$ cell refinement of $Fe_{0.985}S$ just above T_α.

This series of refinements of the LT $\sqrt{3}a,2c$ structures, confirms quantitatively the parallelism of vacancies and temperature in the disorder process. The measure of this disorder is given by the relative reduction of the scale factors versus x and T in Table IV. This shows that the $\sqrt{3}a,2c$ superstructure evolves all the more quickly to short-range order when x and/or T are high.

(B) The LT $\sqrt{3}a,2c$ Lattice: Evolution with x and T

The $\sqrt{3}a,2c$ cell represented in Fig. 6 has been described in Part I. Remember that the Fe atoms shift in the hexagonal plane from their ideal NiAs positions and form contracted and expanded triangular clusters that break the infinite 001 Fe chain of

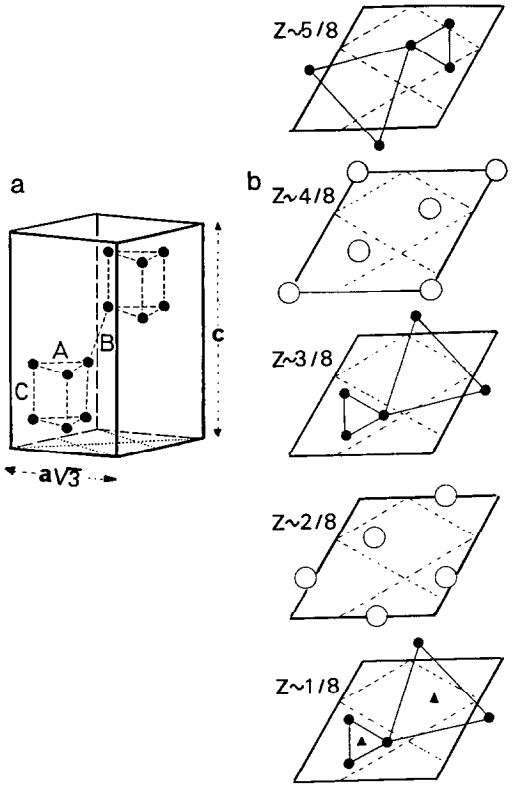

FIG. 6. (a) Schematic Fe–Fe lattice in the LT $\sqrt{3}a,2c$ cell, with characteristic Fe–Fe distances. (b) Alternation of iron (solid circles) and sulfur (open circles) planes in the c direction, from $z = \frac{1}{8}$ to $z = \frac{5}{8}$. In metallic planes, tight and expanded Fe triangular clusters are represented. Ideal NiAs positions of Fe atoms lie at the origin of the substructure cell, in dotted lines.

TABLE III

COORDINATES AND THERMAL PARAMETERS ($Å^2 \times 10^4$) IN $Fe_{0.985}S$ HT $2a,c$ STRUCTURE JUST ABOVE T_α, AT 138°C

	Fe_1	Fe_2	S_1	S_2
Ideal NiAs position	$\frac{1}{2}$ 0 0	0 0 0	$\frac{1}{6}$ $\frac{1}{3}$ $\frac{1}{4}$	$\frac{1}{3}$ $\frac{2}{3}$ $\frac{3}{4}$
Position				
$P6_3mc$ ($y = 2x$)	6c	2a	6c	2b
x	0.5109(7)	0	0.1658(4)	$\frac{1}{3}$
z	0	−0.006(2)	0.2448(14)	0.763(2)
U_{11}	322(10)	353(12)	138(9)	84(12)
U_{22}	214(24)	U_{11}	138(14)	U_{11}
U_{33}	141(6)	367(29)	249(16)	83(29)
$U_{12} = 0.5\ U_{22}$				
U_{13}	−20(0)	0	−1(6)	0
U_{23}	2 U_{13}	0	2 U_{13}	0

Total R: 4.5% (197 reflections)
Partial R and nb of reflections in parenthesis
Substructure: 1.8% (55)
Superstructure: 12.2% (142)
Sub (SC(1)) and superstructure (SC(2)) scale factors:
(SC(1) − SC(2))/SC(1) = 50(± 5)%
Substructure lattice constants: a = 3.480(1) Å, b = 5.821(1) Å

an ideal NiAs cell. Tables V and VI give the change of Fe–Fe, Fe–S, and S–S distances versus x and T. The A($\sqrt{3}a$,2c) distance in the contracted triangular Fe cluster measures the strength of the NiAs lattice distortion. (In an ideal NiAs cell this distance should be a_{NiAs}, about 3.4 Å.) The results obtained confirm that when x and/or T increase, the NiAs lattice distortion relaxes: A($\sqrt{3}a$,2c) in RT FeS is short (2.925 Å), but evolves to the value of 3.014 Å in $Fe_{0.975}S$ just below T_α. As a consequence, Fe atoms come nearer to their ideal chain configuration along the c axis and B($\sqrt{3}a$,2c) and C($\sqrt{3}a$,2c) distances are reduced. This results in an inverted hierarchy of Fe–Fe distances: In RT FeS, C($\sqrt{3}a$,2c) and B($\sqrt{3}a$,2c) are the long Fe–Fe distances and A($\sqrt{3}a$,2c) the short distance (respectively 2.985, 2.949, and 2.925 Å). On the other hand, in $Fe_{0.975}S$ just below T_α, C($\sqrt{3}a$,2c) and B($\sqrt{3}a$,2c) are short distances (resp. 2.940 and 2.913 Å), close to the ideal 2.905-Å value, whereas A($\sqrt{3}a$,2c) is the longest Fe–Fe distance (3.014 Å). Finally, the distorted octahedrons $Fe–S_6$ and prisms $S–Fe_6$ tend to be regular, but the average ⟨Fe–S⟩ distances do not change significantly.

TABLE IV

RELATIVE DECREASE ($SC_{sub} - SC_{super}$)/SC_{sub} OF THE SUPERSTRUCTURE SCALE FACTOR WITH RESPECT TO THE SUBSTRUCTURE SCALE FACTOR, VERSUS x AND T IN LT LATTICE

	RT	Just below T_α
FeS	0	8.8%
$Fe_{0.985}S$	2%	21%
$Fe_{0.975}S$	35%	>60%

(C) *The HT 2a,c Lattice*

The $2a,c$ lattice represented in Fig. 7 has been previously described in Part I. Tables VII and VIII present the Fe–Fe, Fe–S, and

TABLE V

CHARACTERISTIC Fe–Fe AND Fe–S DISTANCES (IN Å) IN LT $\sqrt{3}a,2c$ CELLS, AT ROOM TEMPERATURE, AND JUST BELOW THE TRANSITION

		FeS		$Fe_{0.985}S$		$Fe_{0.975}S$	
Distance	Multiplicity	RT	141°C	RT	116°C	RT	110°C
Fe–Fe							
Along c:							
B	1	2.949	2.947	2.944	2.934	2.916	2.913
C	1	2.985	2.974	2.982	2.974	2.956	2.940
Average		2.967	2.960	2.963	2.954	2.936	2.927
Ideal NiAs value = $c/2$		2.939	2.935	2.936	2.931	2.915	2.905
In basal plane:							
A	2	2.925	2.962	2.933	2.998	2.998	3.014
	2	3.660	3.656	3.658	3.649	3.614	3.647
	2	3.802	3.799	3.795	3.780	3.754	3.774
Average		3.462	3.472	3.462	3.475	3.455	3.478
Ideal NiAs value = a		3.444	3.455	3.444	3.461	3.441	3.464
Fe–S							
$Fe–S_3$	1	2.356	2.361	2.358	2.372	2.362	2.372
$Fe–S_2$	1	2.383	2.390	2.385	2.395	2.396	2.366
$Fe–S_3$	1	2.422	2.426	2.417	2.431	2.417	2.396
$Fe–S_2$	1	2.507	2.513	2.503	2.507	2.486	2.520
$Fe–S_1$	1	2.561	2.560	2.559	2.555	2.534	2.548
$Fe–S_3$	1	2.721	2.713	2.719	2.700	2.679	2.707
Average		2.493	2.494	2.490	2.493	2.479	2.485
Ideal NiAs value		2.472	2.476	2.471	2.478	2.464	2.472

Note. SD < 0.005 Å.

TABLE VI

S–S DISTANCES (Å) IN LT $\sqrt{3}a,2c$ CELLS, AT ROOM TEMPERATURE AND AT A TEMPERATURE JUST BELOW T_α

		FeS		$Fe_{0.985}S$		$Fe_{0.975}S$	
Distance	Multiplicity	RT	141°C	RT	116°C	RT	110°C
In basal plane							
$S_1–S_2$	6	3.452	3.462	3.452	3.467	3.448	3.468
$S_2–S_2$	3	3.477	3.483	3.476	3.486	3.469	3.480
$S_3–S_3$	2	3.421	3.433	3.418	3.440	3.412	3.426
$S_3–S_3$	2	3.442	3.457	3.451	3.460	3.454	3.444
$S_3–S_3$	2	3.469	3.476	3.462	3.482	3.458	3.520
Average		3.454	3.463	3.453	3.468	3.450	3.469
Ideal NiAs value = a		3.444	3.455	3.444	3.461	3.441	3.464
Along c							
$S_1–S_3$	6	3.547	3.550	3.548	3.547	3.532	3.546
$S_2–S_3$	3	3.345	3.360	3.346	3.368	3.338	3.376
$S_2–S_3$	3	3.756	3.741	3.748	3.731	3.716	3.661
Average		3.549	3.550	3.548	3.548	3.530	3.532
Ideal NiAs value = a		3.548	3.549	3.546	3.548	3.528	3.527

Note. SD < 0.010 Å.

TABLE VII

Fe–Fe AND Fe–S DISTANCES (Å) IN HT $2a,c$ CELLS JUST AFTER T_α ($T_\alpha + \Delta T$) AND UP TO T_α ($T_\alpha \ll T$)

Distance	Multiplicity	FeS		$Fe_{0.985}S$
		$T_\alpha + \Delta T = 156°C$	$T_\alpha \ll T = 180°C$	$T_\alpha + \Delta T = 138°C$
Fe–Fe				
Along c				
Fe_1–Fe_1 = B	2	2.922	2.922	2.922
Fe_2–Fe_2 = C	2	2.912	2.910	2.911
Average		2.917	2.916	2.916
Ideal NiAs value = $c/2$		2.912	2.910	2.910
In basal plane				
Fe_1–Fe_1 = A	2	3.275	3.265	3.253
Fe_1–Fe_1	2	3.683	3.708	3.707
Fe_1–Fe_2 = D	2	3.482	3.489	3.483
Average		3.480	3.487	3.481
Ideal NiAs value = a		3.479	3.487	3.480
Fe–S				
Fe_1–S_2	1	2.425	2.438	2.423
Fe_1–S_1	2	2.470	2.455	2.457
Fe_1–S_1	2	2.499	2.522	2.520
Fe_1–S_2	1	2.543	2.539	2.545
Average $\langle Fe_1–S \rangle$		2.484	2.489	2.486
Fe_2–S_1	3	2.471	2.472	2.472
Fe_2–S_1	3	2.492	2.489	2.473
Average $\langle Fe_2–S \rangle$		2.481	2.481	2.473
Ideal NiAs value		2.481	2.484	2.481

Note. SD < 0.010 Å.

TABLE VIII

S–S DISTANCES (Å) IN HT $2a,c$ CELLS, JUST AFTER T_α ($T_\alpha + \Delta T$) AND UP TO T_α ($T_\alpha \ll T$)

Distance	Multiplicity	FeS		$Fe_{0.985}S$
		$T_\alpha + \Delta T = 156°C$	$T_\alpha \ll T = 180°C$	$T_\alpha + \Delta T = 138°C$
In basal plane				
S_1–S_1	2	3.478	3.479	3.462
S_1–S_1	2	3.480	3.494	3.498
S_1–S_2	2	3.481	3.489	3.482
Average		3.480	3.487	3.481
Ideal NiAs value = a		3.479	3.487	3.480
Along c				
S_1–S_2	1	3.441	3.443	3.452
S_1–S_1	4	3.538	3.536	3.531
S_1–S_2	1	3.635	3.641	3.634
Average		3.538	3.538	3.535
Ideal NiAs value		3.537	3.539	3.536

Note. SD < 0.010 Å.

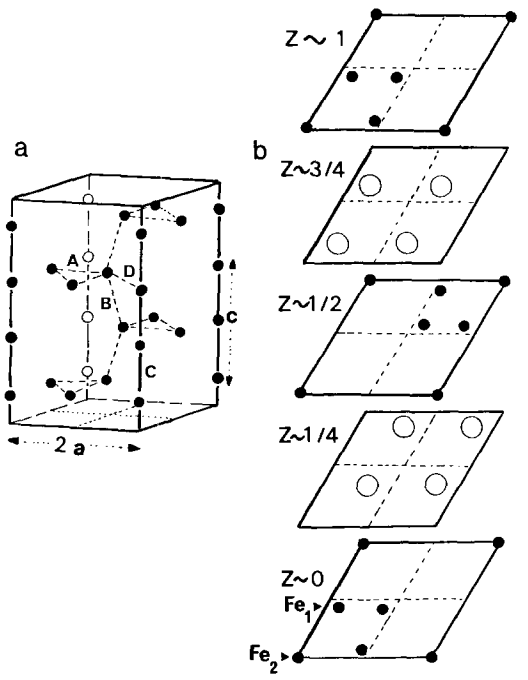

FIG. 7. (a) Schematic Fe–Fe lattice in the hexagonal $2a,c$ HT modification of FeS, with characteristic Fe–Fe distances. (b) Alternation of iron (solid circles) and sulfur (open circles) planes in the c direction, from $z = 0$ to $z = 1$. Ideal NiAs positions of Fe atoms lie at the origin of the substructure cell, in dotted lines.

S–S distances deduced from structural analysis of HT FeS and $Fe_{0.985}S$. One notes that they do not change significantly with x and T.

As pointed out in the previous paper, this HT modification is intermediate between the ideal NiAs and the LT $\sqrt{3}a,2c$ cells. From the former, there remains the infinite Fe chain along the c axis and from the latter, the triangular Fe clusters. The short Fe–Fe distances B($2a,c$) and C($2a,c$), close to 2.92 Å, are along the c axis and the long distance A($2a,c$), in the order of 3.26 Å, is in the cluster of the hexagonal plane. One remarks that the change of the Fe–Fe distances in the LT $\sqrt{3}a,2c$ domains versus x and T makes their distribution closer to that of the HT cell. This explains the lowering of the energy of the transition when x increases.

IV. Discussion

We summarize the physical characteristics of $Fe_{1-x}S$ during the α transition (*6–9*).

For $T < T_\alpha$, the conductivity σ is that of a semiconductor, but the dependence $\sigma = f(T)$ does not fit a classical law. This conductivity is proportional to x.

For $T > T_\alpha$, σ has values on the order of a metallic conductivity, but a weak activation energy remains.

Initially, Townsend *et al.* (*9*) proposed the following band scheme to explain the mechanism of the α transition:

For $T < T_\alpha$, the energy of the sixth electron of Fe^{2+} is split into two subbands separated by a gap at the origin of the thermal activation of the conductivity. At $T > T_\alpha$, these two bands overlap and the conductivity is due to the delocalization of this electron. But four arguments contest this scheme:

—It does not account for the atypic semiconductor behavior of the LT phase.

—Above the transition, antiferromagnetic order remains, with no change in local Fe^{2+} moments.

—The metallic conductivity of the HT phase deduced from this band scheme is incompatible with the existence of a weak activation energy.

—It does not explain the progressive dislocation of the LT lattice in the pretransition process.

Roux-Buisson (*10*) suggests another band scheme which supposes the existence of an impurity level in the band gap of FeS: Mössbauer studies in $Fe_{1-x}S$ establish that cations are always divalent (*11*). Nonstoichiometry supposes that around each vacancy, covalent pairs $(S–S)^{2-}$ are created and give a S^- impurity level populated by electrons from the sulfur band when x in-

creases. The conductivity would originate from holes in the sulfur band. This hypothesis accounts for the p-type conductivity observed in the whole temperature range.

Such covalent pairs $(S–S)^{2-}$ are known to exist in pyrite, FeS_2, where S–S distances are short (2.14 Å). The hypothesis of their formation in the $Fe_{1-x}S$ system is supported when comparing the average ⟨S–S⟩ distances of the extrema of the system: From FeS to Fe_7S_8, this average value decreases from 3.49 to 3.45 Å.

The existence of these vacancy-derived impurity levels in the band gap of FeS makes the band scheme of $Fe_{1-x}S$ identical to the scheme proposed by the authors (*2*) for FeS alloyed with CrS ($Fe_{1-x}Cr_xS$). In chalcogenides, chromium can have two valence states: Cr^{3+} or Cr^{2+} as in CrS which is NiAs type. In $Fe_{1-x}Cr_xS$, the impurity level is populated by the additional carrier brought by Cr^{2+}.

The parallelism of the band schemes is supported by the same behavior of $Fe_{1-x}S$ and $Fe_{1-x}Cr_xS$ with respect to the following transition characteristics:

—Same structural types on both sides of the transition.

—Disappearance of the transition beyond a critical composition x_{lim} equal to 0.05 for $Fe_{1-x}S$ and 0.08 for $Fe_{1-x}Cr_xS$.

—Decrease in T_α and in the transition amplitude, and increase in the hysteresis when x increases.

—Same change of the substructure lattice constants a and c versus x, and, at the transition, the same discontinuity of these parameters with $c_{HT} < c_{LT}$ and $a_{HT} > a_{LT}$.

—Nontypical semiconductor for $T < T_\alpha$ and a bad metal with a weak activation energy for $T > T_\alpha$.

The authors have noted that the previous band scheme proposed for $Fe_{1-x}Cr_xS$ leads to a conduction mechanism referring to a polaron model which identifies the transition as a transition from a nondegenerate polaron gas for $T < T_\alpha$ to a degenerate polaron gas for $T > T_\alpha$. This model, supported by the FeS band scheme involving the S^- impurity level, accounts for the transport properties and structural behavior of $Fe_{1-x}S$ materials around the transition.

The polaron conductivity involves two activation energies:

—The constant hopping energy E_h which corresponds to the gap between impurity level and conduction band.

—The dissociation energy for carriers E_d which accounts for the breaking up of the $\sqrt{3}a,2c$ lattice and coming out of disorder associated with the creation of polarons.

In the case of $Fe_{1-x}M_xS$ (M = Cr, Mn) the fit of the polaron conductivity formula to experimental results establishes that E_d is temperature dependent. This dissociation energy which corresponds to the extraction of a cation from its cluster, decreases with the correlation length of ordered domains, i.e., when x and/or T increase and goes to zero at the transition and when the $\sqrt{3}a,2c$ lattice has disappeared. At $T > T_\alpha$, there remains only the hopping term E_h which explains the slight increase in T observed for the HT phase.

The nondegenerate polaron gas conductivity ($T < T_\alpha$) is proportional to the number of carriers which for $Fe_{1-x}S$ materials is given by twice the number of vacancies (one vacancy populates two S^- impurity levels). This agrees with the linear dependence $\sigma = f(x)$ observed at a given T in the LT phase.

In the polaron theory, Mott (*12*) predicts that for an impurity-induced transition, there is a critical polaron concentration between 0.07 and 0.1, beyond which the α transition disappears, when two polarons compete for the same site. Beyond this concentration, the polaron gas becomes degen-

erate, i.e., corresponds to the HT phase. Precisely, in $Fe_{1-x}S$ and $Fe_{1-x}Cr_xS$ systems, the transition can be x-induced. In the case of $Fe_{1-x}Cr_xS$, the critical concentration $x_{crit}(= x_{lim})$ is equal to 0.08. In these materials, there is one polaron per chromium, but for $Fe_{1-x}S$ they are two per vacancy. Under those conditions, x_{crit} must be half the previous value, what is approximately observed with $x_{crit} = x_{lim} = 0.05$.

The study of $Fe_{1-x}Mn_xS$ materials ($x < 0.12$), which also exhibit a transition, provides the possibility of extending to stoichiometric FeS the previous polaron model (*2*). Substitution with Mn^{2+} atoms does not bring impurity carriers (MnS is an insulator with a large gap), and S^- impurity levels are supposed to be populated by thermal activation only. The fit of the polaron conductivity to experimental results obtained on $Fe_{1-x}Mn_xS$ confirms the validity of this assumption.

In conclusion, one remarks the interest, for the study of the α transition in purely iron-defective compounds $Fe_{1-x}S$, in substituting vacancies by Cr^{2+}, Mn^{2+}, and Co^{2+} ions. The whole set of simultaneous structural and physical analyses converges to a global discussion of the α transition in NiAs-type compounds.

References

1. F. KELLER-BESREST AND G. COLLIN, submitted for publication.
2. G. COLLIN, M. F. GARDETTE, G. KELLER, AND R. COMES, *J. Phys. Chem. Solids* **46**(7), 809–821 (1985).
3. G. COLLIN, M. F. GARDETTE, AND R. COMES, *J. Phys. Chem. Solids* **48**(9), 791–802 (1987).
4. F. KELLER-BESREST, Thèse d'Etat, Université Paris 6 (1984).
5. F. KELLER-BESREST AND G. COLLIN, *Acta. Crystallogr. B* **38**, 296–303 (1982).
6. W. MOLDENHAUER AND W. BRUCKNER, *Phys. Status Solidi A* **34**, 565–571 (1976).
7. J. MOLENDA, S. MROWEC, AND A. STOKLOSA, *Solid State Ionics* **1**, 273–286 (1980).
8. J. M. COEY, H. ROUX-BUISSON, AND R. BRUSETTI, *J. Phys. Paris* **37** (Suppl. No. 10), C4 1–10 (1976).
9. M. G. TOWNSEND, J. R. GOSSELIN, R. J. TREMBLAY, AND A. H. WEBSTER *J. Phys. Paris* **37** (Suppl. No. 10), C4 11–16 (1976).
10. H. ROUX-BUISSON, Thèse d'Etat, Université Grenoble I (1980).
11. G. N. GONCHAROV, Y. M. OSTANEVICH, S. B. TOMILOV, AND L. CSER, *Phys. Status Solidi* **37**, 141–149 (1970).
12. N. F. MOTT, "Metal–Insulator transitions," Taylor and Francis, London (1974).